ACS OMEGA

http://pubs.acs.org/journal/acsodf

Article

Selective Hydrogenation of Dimethyl Oxalate to Methyl Glycolate over Boron-Modified Ag/SiO_2 Catalysts

Shuai Cheng, Tao Meng,* Dongsen Mao,* Xiaoming Guo, and Jun Yu

Cite This: *ACS Omega* 2022, 7, 41224−41235

Read Online

ACCESS | Metrics & More | Article Recommendations | Supporting Information

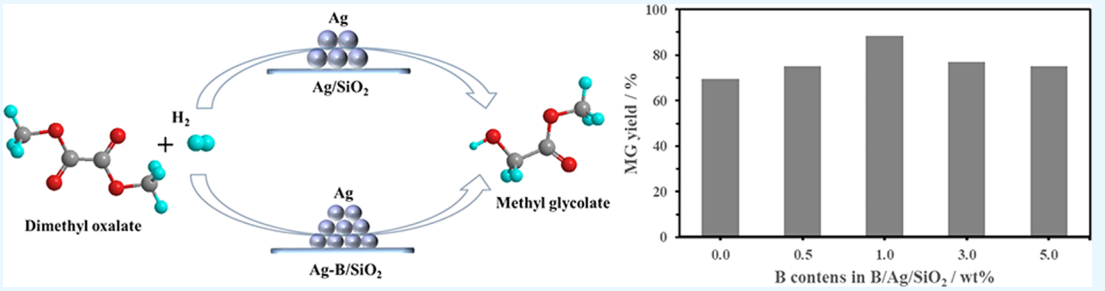

ABSTRACT: The addition of boron (B) as a promoter to the Ag/SiO_2 catalyst for the selective hydrogenation of dimethyl oxalate (DMO) to methyl glycolate (MG) was investigated. A comparison of the preparation method for incorporation of B found that the addition during the ammonia evaporation deposition−precipitation synthesis of the Ag/SiO_2 catalyst ($Ag-B/SiO_2$) was inferior to incipient wetness impregnation introduction of the Ag/SiO_2 catalyst ($B/Ag/SiO_2$). Moreover, the effects of B contents (0.5−5 wt %) on the physicochemical properties and catalytic performance of the $B/Ag/SiO_2$ catalysts were investigated by XRF, N_2-physisorption, XRD, FTIR, TEM, EDX mapping, H_2-TPR, NH_3-TPD, XPS, and catalytic testing. The results indicated that both the catalytic activity and stability of the Ag/SiO_2 catalyst were noticeably enhanced after the introduction of B. The $B/Ag/SiO_2$ catalyst with 1 wt % B showed the best catalytic performance of 100% DMO conversion and 88.3% MG selectivity, which could be attributed to the highest dispersion of the active metal and the smallest Ag particle size stabilized by the strong interaction between silver and boron species.

1. INTRODUCTION

Recently, catalytic conversion of synthetic gas to produce dimethyl oxalate (DMO) and further hydrogenation of DMO to ethylene glycol (EG) have been successfully scaled up to industrial applications.[1] Unfortunately, the production of methyl glycolate (MG), which is a more intermediate product in the hydrogenation of DMO to EG, has not received enough attention. Actually, MG is an important and higher value-added fine chemical in comparison with EG. Because of its α-H, hydroxyl, and ester groups, MG exhibits similar chemical properties to those of alcohol and ester,[2−6] and it can be used for the synthesis of numerous fine chemicals, such as polyglycolic acid, pharmaceuticals, and perfumes.[4,7] More importantly, these MG-derived products are environmentally friendly and biodegradable. Thus, MG possesses an extensive potential market.

Currently, there are several methods to produce MG; however, some disadvantages of these approaches, such as the limited raw materials, harsh reaction conditions, and low yield of the target product, impede their applications in the industry.[4,8,9] The selective hydrogenation of DMO is a more efficient and greener catalytic procedure for MG synthesis.[3,10−12] However, low activity and poor stability of the catalyst are common problems.[13,14] Therefore, effective catalysts particularly with high reactivity and stability are urgently needed.

Based on the available literatures, the catalysts used in the hydrogenation of DMO reactions are mainly noble metal-free based[3,8,15−20] and silver-based[1,11,21−26] catalysts. Among noble metal-free based catalysts, copper-based catalysts are usually preferred for the synthesis of EG and ethanol.[15−18] Cu/HAP catalysts showed distinct catalytic performance because of the copper phosphate species and abundant surface hydroxy groups.[27] Abbas et al.[28] found that Cu nanoparticles wrapped on reduced graphene oxide (RGO) nanosheets possessed a synergistic ratio of $Cu^+/(Cu^+ + Cu^0)$ and highly dispersed Cu nanoparticles, which were in favor of catalytic performance in hydrogenation of DMO. Zhao et al. reported that Ni_3P/RB-MSN showed better catalytic performance than Ni_3P/HMS

Received: August 1, 2022
Accepted: September 22, 2022
Published: October 31, 2022

and Ni_3P/MCM-41, which was due to the lack of Si−OH in the RB-MSN.[29] As a unilateral hydrogenated product, MG has an inferior yield because of the higher thermodynamic constant of the subsequent hydrogenation of MG to EG.[3] Recently, several silver-based catalysts, such as Ag/SiO_2,[21] Ag/MCM-41,[22] Ag/KCC-1,[1,26] Ag/SBA-15,[24] and Ag/CNT,[25] have been investigated and exhibited superior selectivity for the chemoselective synthesis of MG via hydrogenation of DMO due to the relatively weak hydrogenolysis capability of the silver active sites compared with copper. However, these catalysts have the disadvantages of high raw material cost, complex preparation process, and poor stability, thus impeding their further industrial application.[30]

On the other hand, it has been well demonstrated that the catalytic activity and stability of metal catalysts can be improved by introducing an effective promoter due to the enhanced dispersion of the active metal and interaction between the metal and dopant.[13,31] Recently, many studies have shown that B_2O_3 is a promising candidate for its sintering-resistant property and suitable acidity. For instance, He et al.[32] claimed that the catalytic behavior was greatly enhanced with the B_2O_3-modified Cu−SiO_2 catalyst due to the improved copper dispersion. Moreover, boron doping could enhance the metal−support interaction between Cu and SiO_2, maintain a suitable Cu^+/Cu^0 ratio, restrain the growth of Cu particles during DMO hydrogenation, and then improve the catalytic selectivity and stability of Cu/SiO_2 catalysts.[33,34] Yin et al.[35] reported that the Cu/HMS catalyst modified by B_2O_3 exhibited higher conversion and selectivity because of the higher metallic copper surface area and copper dispersion. More recently, Chen et al.[30] demonstrated that a 10%Ag−5% B_2O_3/SiO_2 catalyst prepared by the coimpregnation method displayed an improved catalytic activity and stability compared with the Ag/SiO_2 catalyst in the hydrogenation process. However, inhomogeneous agglomeration of active species usually occurs especially at high content for the catalyst prepared by the impregnation method, resulting in large-sized particles and thus low activity and poor stability.[36,37] In previous work,[38] we found that the addition of 1 wt % B exerted little effect on the DMO conversion and MG selectivity of the 10%Ag/SiO_2 catalyst prepared by the one-step ammonia evaporation deposition−precipitation method. The above results[30,38] indicated that the effect of B addition on the catalytic performance of Ag/SiO_2 may depend greatly on the catalyst preparation method and B_2O_3 content, which has not been investigated so far to the authors' best knowledge.

In the present work, we report a series of B-modified Ag/SiO_2 catalysts with different boron loadings for the selective hydrogenation of DMO to MG. The Ag/SiO_2 catalyst was synthesized by a facile ammonia evaporation deposition−precipitation method, which was reported superior to the impregnation method for the preparation of the Cu/SiO_2 catalyst.[39] The B promoter was incorporated through two methods, i.e., addition during the ammonia evaporation deposition−precipitation synthesis of the Ag/SiO_2 catalyst (Ag−B/SiO_2) and incipient wetness impregnation after the synthesis of the Ag/SiO_2 catalyst (B/Ag/SiO_2). Comprehensive characterization was performed by XRF, N_2-physisorption, XRD, FTIR, TEM, EDX mapping, H_2-TPR, XPS surface analysis, and NH_3-TPD techniques, and the effects of boron loadings on the physicochemical properties of the B/Ag/SiO_2 catalysts were investigated. Moreover, the structure−activity relationship of these B/Ag/SiO_2 catalysts in DMO hydrogenation was also discussed in detail.

2. RESULTS AND DISCUSSION

2.1. Effect of B Incorporation Order on Catalytic Performance of Ag/SiO_2. The effect of incorporation order of B on the catalytic performance of Ag/SiO_2 modified with 1% B was investigated, and the results are presented in Figure 1. It can be observed that the DMO conversion of the 1B/Ag/

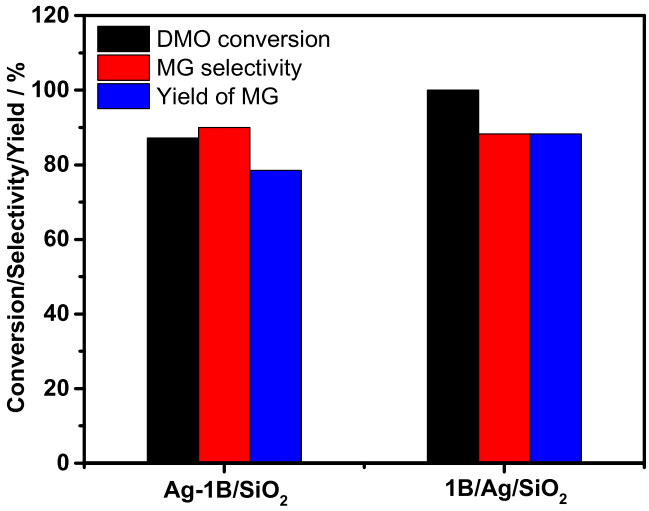

Figure 1. Comparison of performance of 1% B-modified Ag/SiO_2 catalyst prepared by one-step ammonia evaporation deposition−precipitation and postincipient wetness impregnation.

SiO_2 catalyst was significantly higher than that of the Ag−1B/SiO_2 catalyst (88.3 vs 78.5%). At variance with the DMO conversion, similar MG selectivity was obtained on both catalysts. Thus, the $1B/Ag/SiO_2$ catalyst exhibited noticeably higher MG yield than the Ag−1B/SiO_2 catalyst. It was reported that the introduced B can be removed to a large extent during washing of the precipitate for the B-modified Cu−ZnO−ZrO_2 catalyst.[40] And Witoon et al.[41] found that K species were removed during washing and filtration stages for the preparation of Fe−Co−K−Al mixed oxide catalysts. Thus, we speculate that the inferior activity of the Ag−1B/SiO_2 catalyst may be due to the loss of B during the preparation process. To verify the hypothesis, the actual B content of both B-modified catalysts was determined. As expected, the result indicated that the actual B loading of the Ag−1B/SiO_2 catalyst (0.57 wt %) was distinctly lower than that of the $1B/Ag/SiO_2$ catalyst (0.85 wt %). Thus, it can be concluded that the different methods of introducing B had an obvious influence on the actual B content and further affected the catalytic behaviors of the B-modified catalysts. Accordingly, the Ag/SiO_2 catalysts modified with different B loadings were prepared by the postincipient wetness impregnation method to investigate the effect of B content on the performance of the *x*B/Ag/SiO_2 catalyst for hydrogenation of DMO to synthesize MG.

2.2. Effect of B Content on the *x*B/Ag/SiO_2 Catalysts. *2.2.1. Characterization of the xB/Ag/SiO_2 Catalysts.* The composition of the as-prepared *x*B/Ag/SiO_2 catalysts was determined by XRF, and the results are presented in Table 1. As seen, the actual silver loading is in close agreement with the as-added amount. Nevertheless, the actual B loadings were

https://doi.org/10.1021/acsomega.2c04880
ACS Omega 2022, 7, 41224−41235

Table 1. Physicochemical Properties of the Calcined Ag/SiO_2 and xB/Ag/SiO_2 Catalysts

catalyst	Ag loading[a] (wt %)	B loading[a] (wt %)	S_{BET}[b] ($m^2 \cdot g^{-1}$)	V_p[c] ($cm^3 \cdot g^{-1}$)	D_p[d] (nm)
Ag/SiO_2	9.8		179.4	0.65	10.6
0.5B/Ag/SiO_2	9.7	0.42	161.9	0.59	12.2
1B/Ag/SiO_2	9.7	0.85	152.3	0.58	12.4
3B/Ag/SiO_2	9.7	2.8	143.6	0.54	12.4
5B/Ag/SiO_2	9.7	4.7	123.4	0.50	13.0

[a]Determined by XRF. [b]BET specific surface area. [c]Pore volume. [d]Average pore diameter.

slightly lower than the theoretical values, indicating that a small amount of B was lost during the catalyst preparation; a similar phenomenon was also reported previously for the B-modified Cu−SiO_2 catalyst.[32]

To explore the effect of B content on the textural properties of xB/Ag/SiO_2 catalysts, N_2 adsorption−desorption measurements were carried out. The values of the BET surface area (S_{BET}), pore volume (V_p), and pore diameter (D_p) of the as-prepared samples are summarized in Table 1. The results showed that the S_{BET} and V_p decreased obviously and continuously with increasing B content, while the D_p enlarged slightly of the xB/Ag/SiO_2 catalysts compared with the parent Ag/SiO_2 catalyst. Specifically, the S_{BET} and V_p decreased from 179.4 $m^2 \cdot g^{-1}$ and 0.65 $cm^3 \cdot g^{-1}$ of the Ag/SiO_2 catalyst to 123.4 $m^2 \cdot g^{-1}$ and 0.50 $cm^3 \cdot g^{-1}$ of the 5B/Ag/SiO_2 catalyst, respectively. This phenomenon was probably caused by boria molecules entered into and plugged some pores of the Ag/SiO_2 catalyst during the process of impregnation.[32]

Figure 2 shows the N_2 adsorption−desorption isotherms and BJH pore size distributions of the catalysts. As can be seen from Figure 2A, all of the samples exhibited a typical adsorption curve of type IV with the H1-type hysteresis loop, which is the characteristic of nanostructured materials with uniform mesopores. The pore size distributions of different samples (Figure 2B), derived from desorption data of the isotherm and calculated using the BJH model, show that most of the pores fall into the size range of 2−20 nm and the average pore size is calculated to be about 12 nm.

To investigate the evolution of the crystalline phase structure of the xB/Ag/SiO_2 catalysts, the XRD patterns of both calcined and reduced catalysts were collected. As shown in Figure 3A, for all of the catalysts, four peaks appeared at 2θ = 38.1, 44.3, 64.4, and 77.4°, which were assigned to the (111), (200), (220), and (311) lattice planes of metallic silver (PDF # 87-0597).[33] The appearance of the characteristic diffraction peaks of metallic silver in the calcined catalysts can be ascribed to the fact that silver oxide is easily decomposed into metallic silver during the heat treatment at high temperatures.[30] With the addition of B, the intensity of the diffraction peak of Ag decreased noticeably, and the characteristic peaks of B_2O_3 emerged at 2θ of 14.6 and 27.8° (PDF # 06-0297)[33] when the doping amount of B was greater than or equal to 3 wt % in the xB/Ag/SiO_2 catalyst. Additionally, a broad and diffuse diffraction peak centered at about 22° was observed for all of the catalysts, which was assigned to amorphous SiO_2.[42]

The XRD patterns of the reduced catalysts are shown in Figure 3B, and the average diameter of metallic Ag was calculated by the Scherrer equation. From calculations, the average diameters of metallic Ag on Ag/SiO_2, 0.5B/Ag/SiO_2, 1B/Ag/SiO_2, 3B/Ag/SiO_2, and 5B/Ag/SiO_2 are 16.9, 14.7, 13.2, 13.6, and 13.7 nm, respectively. It is clear that the crystalline sizes of silver in the xB/Ag/SiO_2 catalysts are smaller than that in the Ag/SiO_2 catalyst. It can be inferred that the Ag particles aggregated on the support surface due to the weak interaction between silver species and silica support, and the introduction of B could suppress the accumulation of silver species and retard the growth of metallic silver crystallites during the calcination and reduction processes.[30] Specifically, B_2O_3 doping with a B loading no higher than 1 wt % notably decreased the particle size of Ag from 14.7 to 13.2 nm, whereas further increasing B loading in the range of 1−5 wt % resulted in a gradual increase in the particle size of Ag from 13.2 to 13.7 nm. Evidently, the 1B/Ag/SiO_2 catalyst exhibited the smallest particle size among all of the catalysts. The results clearly demonstrated that the introduction of proper amounts of B in

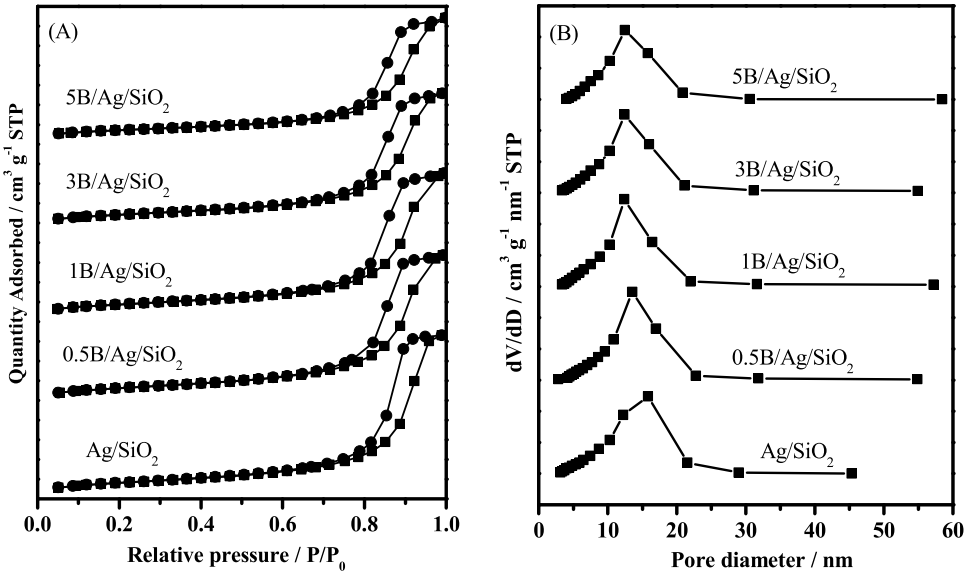

Figure 2. N_2 adsorption isotherms (A) and BJH pore size distributions (B) of the calcined Ag/SiO_2 and xB/Ag/SiO_2 catalysts.

https://doi.org/10.1021/acsomega.2c04880
ACS Omega 2022, 7, 41224−41235

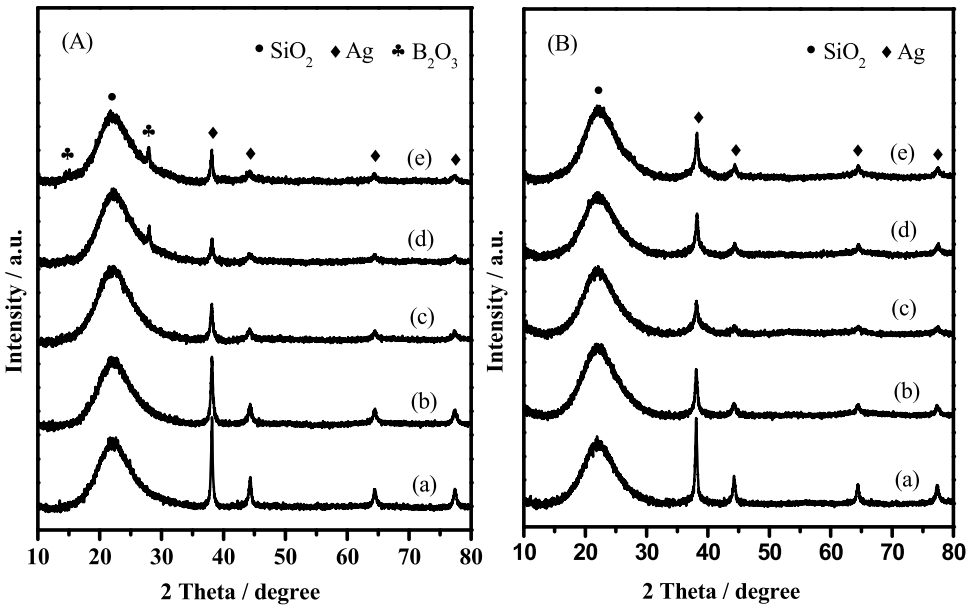

Figure 3. XRD patterns of different catalysts upon (A) calcination and (B) reduction: (a) Ag/SiO_2, (b) $0.5B/Ag/SiO_2$, (c) $1B/Ag/SiO_2$, (d) $3B/Ag/SiO_2$, and (e) $5B/Ag/SiO_2$.

the xB/Ag/SiO_2 catalysts could enhance the dispersion of the silver.

The FTIR technique was adopted to further explore the structure information of the calcined samples. As shown in Figure 4, the absorption bands at approximately 1100, 800, and

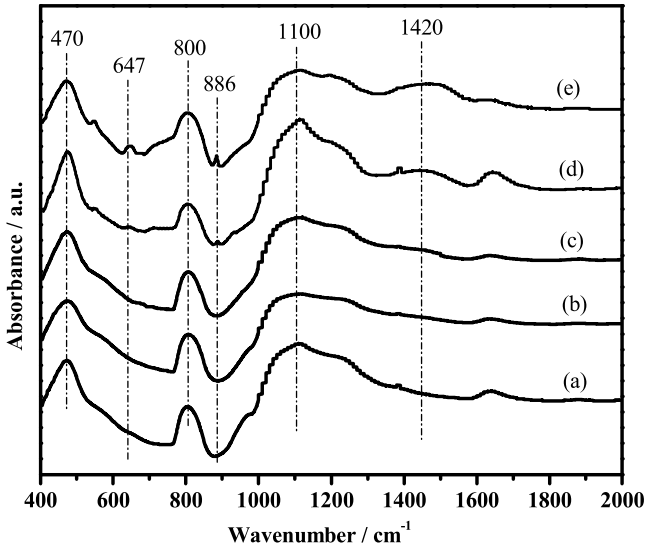

Figure 4. FTIR spectra of different catalysts after calcination: (a) Ag/SiO_2, (b) $0.5B/Ag/SiO_2$, (c) $1B/Ag/SiO_2$, (d) $3B/Ag/SiO_2$, and (e) $5B/Ag/SiO_2$.

470 cm^{-1} on the Ag/SiO_2 catalyst were ascribed to the different vibration modes of the Si−O bonds of the SiO_2 support.[43,44] In addition, the bands at approximately 1420, 886, and 647 cm^{-1} appeared with the samples of $3B/Ag/SiO_2$ and $5B/Ag/SiO_2$, which were assigned to the B−O stretching vibrations of trigonal (BO_3) units in different borate groups, the stretching vibrations of B−O bonds in BO_4 units from diborate groups, and the B−O−B bending vibrations, respectively.[43,45] Furthermore, the intensity of these bands increased noticeably with increasing the boron content. The result is in good accordance with that obtained by XRD (Figure 3A).

Figure 5 shows TEM images of the two representative catalysts (calcined Ag/SiO_2 and $1B/Ag/SiO_2$). According to our group's previous study[38,46] and the above XRD results (Figure 3), Ag species mainly exist as metallic Ag on calcined catalysts. Both calcined Ag/SiO_2 and $1B/Ag/SiO_2$ appear as agglomerates of irregular SiO_2 support (bright areas) and spherical Ag species particles (darker areas). However, the average Ag particle size of $1B/Ag/SiO_2$ (5−10 nm) is obviously smaller than that of Ag/SiO_2 (10−20 nm). The dispersion of Ag species was further investigated by EDX mapping (Figure 6). Obviously, Ag species are better dispersed on $1B/Ag/SiO_2$ (Figure 6a) than on Ag/SiO_2 (Figure 6b). Besides, the B species on $1B/Ag/SiO_2$ is also highly dispersed (Figure S1). The results of TEM and EDX mapping implied that B loading could limit the growth of Ag particles and promote the dispersion of Ag species on the SiO_2 support.

As displayed in Figure 7, all of the samples exhibited one hydrogen consumption peak in the region of 100−300 °C of the TPR profiles. The peak at 137 °C of the Ag/SiO_2 catalyst corresponded to the reduction of silver oxide to metallic silver.[24] However, the calcined catalysts did not show any characteristic diffraction peaks of silver oxides (Figure 3A), which is probably because the XRD technique cannot detect the thin layer of silver oxides on the catalyst surface.[38] The xB/Ag/SiO_2 catalysts exhibited a higher reduction temperature and the H_2 consumption peak gradually shifted toward a higher temperature with increasing B amount. This phenomenon may be attributed to the strong chemical interaction between the acidic boric oxide and the basic silver oxide.[30] With the increase of B content, gaining electrons became harder for the silver species during hydrogen reduction, which was due to the higher electron affinity of boric oxide than that of SiO_2.[32] From the H_2-TPR results, it can be concluded that the amount of B plays a very important role in the distributions of silver species by chemical interaction between boric oxide and Ag species in the xB/Ag/SiO_2 catalysts.

https://doi.org/10.1021/acsomega.2c04880
ACS Omega 2022, 7, 41224−41235

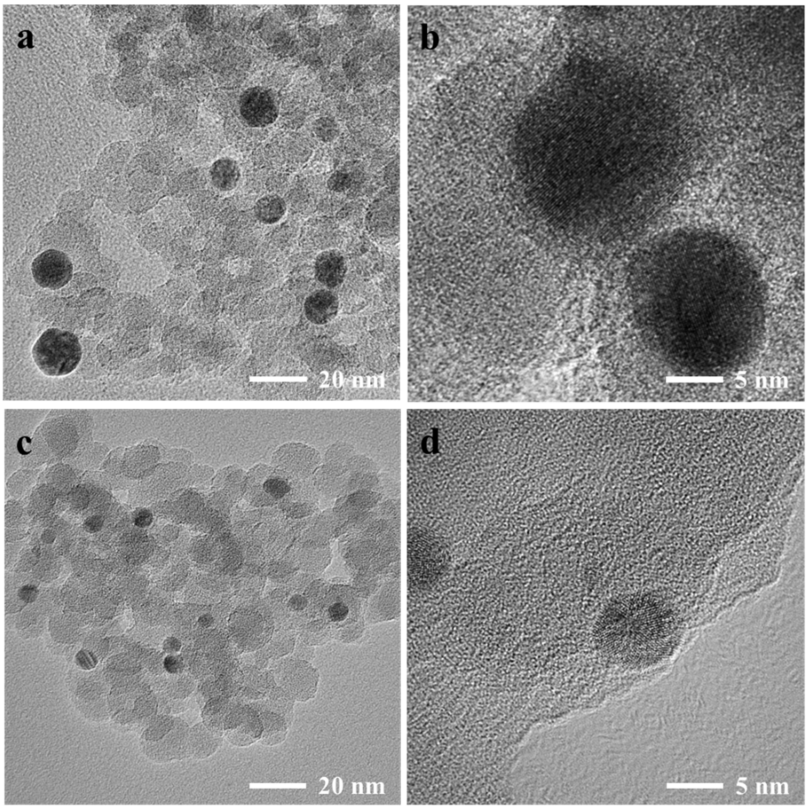

Figure 5. TEM images of the calcined Ag/SiO_2 (a, b) and $1B/Ag/SiO_2$ (c, d).

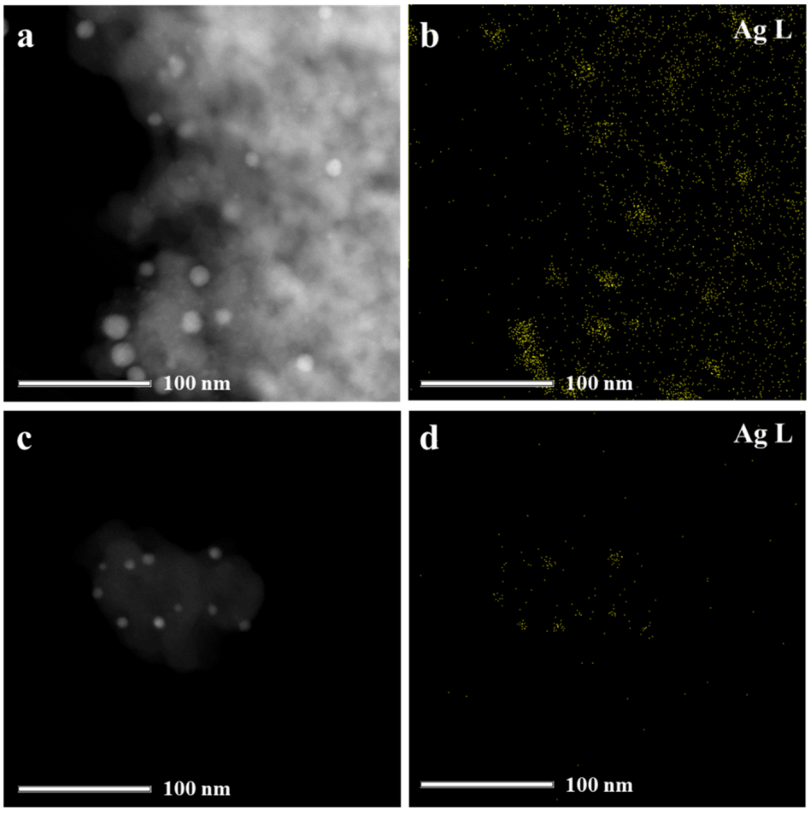

Figure 6. STEM and EDX mapping images of calcined Ag/SiO_2 (a, b) and $1B/Ag/SiO_2$ (c, d).

The NH_3-TPD profiles are shown in Figure 8. As observed, the profile of the Ag/SiO_2 catalyst presented a broad and weak peak centered at 150 °C, indicating that only a small amount of acidic sites existed on the catalyst surface. For the xB/Ag/SiO_2

https://doi.org/10.1021/acsomega.2c04880
ACS Omega 2022, 7, 41224−41235

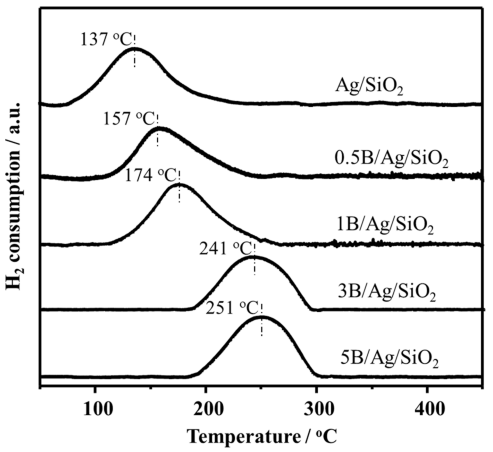

Figure 7. TPR profiles of the as-calcined Ag/SiO_2 and $xB/Ag/SiO_2$ catalysts.

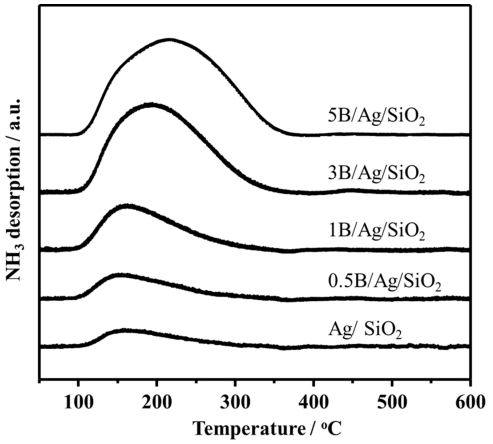

Figure 8. NH_3-TPD profiles of the Ag/SiO_2 and $xB/Ag/SiO_2$ catalysts.

catalysts, the NH_3 desorption temperature shifted toward a higher temperature with an increase in B loading. In addition, the NH_3 desorption peak area also increased gradually with the enhancement of B content. Therefore, it can be inferred that boria was mainly responsible for the acidity of the $xB/Ag/SiO_2$ catalysts.[30,35,36]

The chemical states and surface compositions of the reduced catalysts were investigated using an XPS technique. The XPS spectra of Ag 3d for the Ag/SiO_2 and $xB/Ag/SiO_2$ catalysts are illustrated in Figure 9A. Typically, the two peaks located at binding energies (BEs) of 367.8 and 373.9 eV were mainly ascribed to Ag $3d_{5/2}$ and Ag $3d_{3/2}$ peaks of Ag^0, respectively. As shown in Figure 9B, the B 1s peak centered at about 193.4 eV was attributed to B^{3+},[47] and the absence of a peak at 188.7 eV suggested that no B^0 existed.[48]

The XPS results are summarized in Table 2. As can be seen, the BE values of Ag $3d_{5/2}$ of the $xB/Ag/SiO_2$ catalysts were higher than that of the Ag/SiO_2 catalyst. And the Ag $3d_{5/2}$ peak shifted to higher BEs from 368.0 to 368.3 eV with the increase of B content, while the B 1s peak moved to lower BEs from 193.4 to 192.7 eV. Therefore, an electron donor−acceptor interaction between silver and boria may occur on the silica surface. The experimental results clarified the presence of strong interaction between Ag and B species wherein the electron transferred from Ag^0 to B^{3+}.[30] Additionally, the surface concentration of Ag over the Ag/SiO_2 and $xB/Ag/SiO_2$ catalysts (Table 2) shows a volcano-type tendency, in which the highest amount of surface silver was obtained on the 1B/

Table 2. XPS Results for the Ag/SiO_2 and $xB/Ag/SiO_2$ Catalysts

	binding energy (eV)		surface elemental concentration (at %)	
catalyst	Ag $3d_{5/2}$	B 1s	Ag	B
Ag/SiO_2	367.8		0.53	
$0.5B/Ag/SiO_2$	368.0	193.4	0.56	6.74
$1B/Ag/SiO_2$	368.1	193.3	0.78	10.53
$3B/Ag/SiO_2$	368.2	193.2	0.67	11.99
$5B/Ag/SiO_2$	368.3	192.7	0.60	13.35

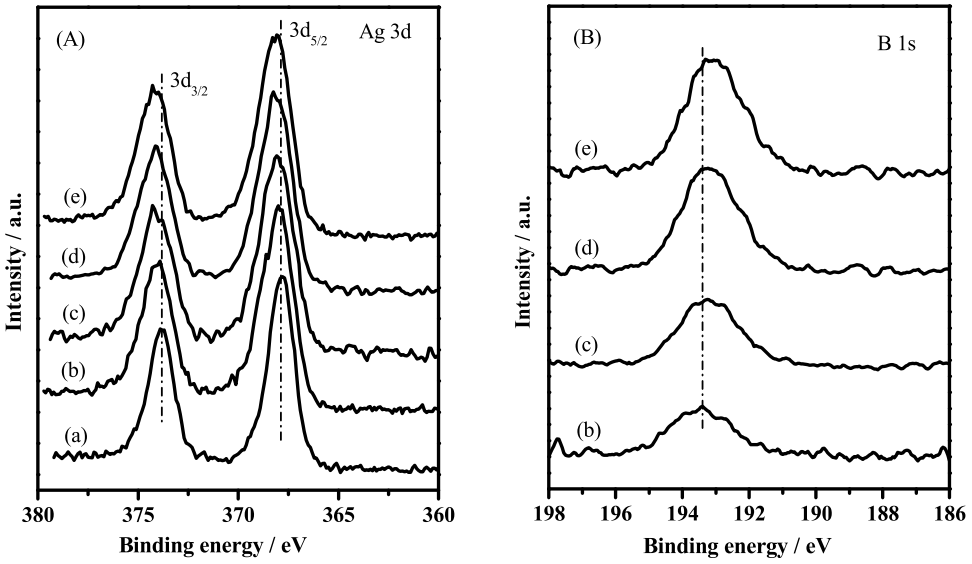

Figure 9. Ag 3d (A) and B 1s (B) photoelectron spectra of the reduced catalysts: (a) Ag/SiO_2, (b) $0.5B/Ag/SiO_2$, (c) $1B/Ag/SiO_2$, (d) $3B/Ag/SiO_2$, and (e) $5B/Ag/SiO_2$.

https://doi.org/10.1021/acsomega.2c04880
ACS Omega 2022, 7, 41224−41235

Ag/SiO_2 catalyst. This result is in good agreement with the dispersion of Ag obtained from XRD measurements (Table 1).

2.2.2. Catalytic Performance of the xB/Ag/SiO$_2$ Catalysts. The results of Ag/SiO_2 and xB/Ag/SiO_2 catalysts for the selective hydrogenation of DMO to MG are listed in Table 3.

Table 3. Catalytic Performance of the Ag/SiO_2 and xB/Ag/SiO_2 Catalysts for DMO Hydrogenation[a]

		selectivity (%)			
catalyst	conversion (%)	MG	MF	EG	MG yield (%)
Ag/SiO_2	77.8	89.3	2.2	8.5	69.5
$0.5B/Ag/SiO_2$	79.4	94.5	5.5	0	75.0
$1B/Ag/SiO_2$	100	88.3	2.4	9.3	88.3
$3B/Ag/SiO_2$	88.0	87.5	3.8	8.7	77.0
$5B/Ag/SiO_2$	89.7	83.7	5.3	11.0	75.1

[a]Reaction conditions: T = 493 K, P = 1.5 MPa, H_2/DMO molar ratio = 150, LHSV = 0.28 h^{-1}.

The products of DMO hydrogenation reaction on the silver-based catalyst include EG and methyl formate (MF) besides the target product of MG. Under the present reaction conditions, the conversion of DMO and the selectivity to MG on the Ag/SiO_2 catalyst are 77.8 and 89.3%, respectively. As B was introduced into the Ag/SiO_2 catalyst, both the catalytic activity and the selectivity of MG were improved. And along with the increase of the B loading, the catalytic performance displayed a volcano-type variation tendency in terms of MG yield. More specifically, the highest yield of MG was observed on the $1B/Ag/SiO_2$ catalyst (88.3%); the value was 18.8% higher than that on the unmodified Ag/SiO_2 catalyst.

The TOF was calculated to compare the catalytic performance of different catalysts in DMO hydrogenation, and the DMO conversion was regulated by DMO liquid hourly space velocity (LHSV).[24] As shown in Table 4, both the TOF and D_{Ag} values increased first and then decreased with increasing the content of B. $1B/Ag/SiO_2$ with the highest TOF value (17.8 h^{-1}) indicated its highest DMO catalytic activity. Besides, the addition of B promoted the dispersion of Ag species on SiO_2, consistent with TEM results (Figure 5). Figure 10 shows that the TOF value decreased gradually with the increase of Ag particle size over five catalysts, suggesting that the DMO hydrogenation is a structure-sensitive reaction.[46]

As well known, there are many factors that can affect the activity of Ag-based catalysts for vapor-phase DMO hydrogenation. On the basis of the above characterization results, the reasons for the effect of B loading on the performance of the

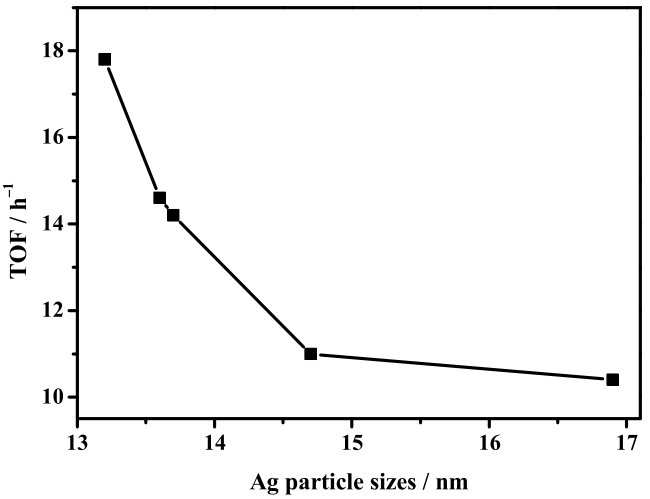

Figure 10. TOF values as a function of Ag particle sizes of the Ag/SiO_2 and xB/Ag/SiO_2 catalysts.

xB/Ag/SiO_2 catalysts can be explained as follows: (1) The XPS results show that the surface Ag content increased in the order of Ag/SiO_2 < $0.5B/Ag/SiO_2$ < $5B/Ag/SiO_2$ < $3B/Ag/SiO_2$ < $1B/Ag/SiO_2$ (Table 2). This order exactly coincided with that of MG yield of the series of catalysts. In fact, the MG yield increased almost linearly with the surface Ag content of the catalysts, as shown in Figure 11. Thus, the surface metallic

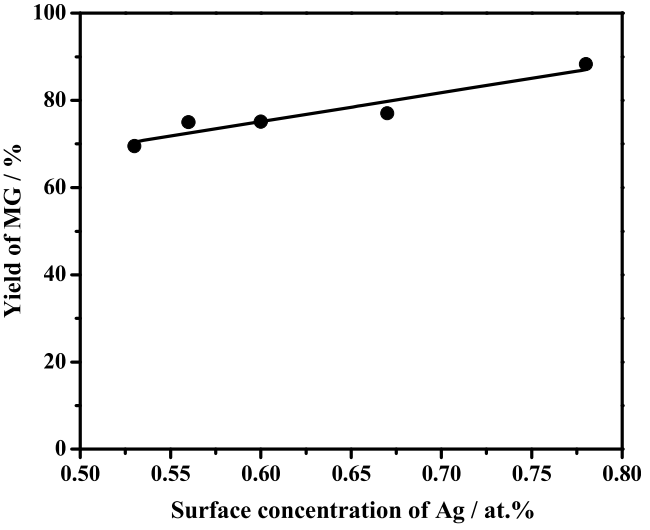

Figure 11. Relationship between the MG yield and the surface Ag concentration of the Ag/SiO_2 and xB/Ag/SiO_2 catalysts.

Table 4. TOF of the Ag/SiO_2 and xB/Ag/SiO_2 Catalysts for DMO Hydrogenation[a]

		selectivity (%)				
catalyst	conversion (%)	MG	others[b]	d_{Ag}[c] (nm)	D_{Ag}[d] (%)	TOF_{XRD}[e] (h^{-1})
Ag/SiO_2[f]	15.7	91.9	8.1	16.9	9.00	10.4
$0.5B/Ag/SiO_2$[f]	19.6	96.8	3.2	14.7	10.35	11.0
$1B/Ag/SiO_2$[g]	11.7	100	0	13.2	11.52	17.8
$3B/Ag/SiO_2$[g]	9.3	99.4	0.6	13.6	11.18	14.6
$5B/Ag/SiO_2$[g]	9	98.9	1.1	13.7	11.10	14.2

[a]Reaction conditions: T = 493 K, P = 1.5 MPa, H_2/DMO molar ratio = 150. [b]Others include EG and MF. [c]Average diameter of metallic Ag on the reduced catalysts calculated by the Scherrer equation. [d]Dispersion of metallic Ag determined by XRD. [e]TOFXRD was calculated by Ag dispersion. [f]LHSV = 0.58 h^{-1}. [g]LHSV = 1.75 h^{-1}.

https://doi.org/10.1021/acsomega.2c04880
ACS Omega 2022, 7, 41224−41235

Ag site density was mainly responsible for the catalytic activity, which can offer a rational explanation for the boron content effect on the catalytic performance of the xB/Ag/SiO_2 catalysts. (2) It has been well illustrated that the dispersion and particle size of metallic Ag have a significant effect on the catalytic performance of the Ag-based catalysts.[23,30,49] As revealed by XRD measurements, the particle size of silver species decreased in the following order: Ag/SiO_2 > 0.5B/Ag/SiO_2 > 5B/Ag/SiO_2 > 3B/Ag/SiO_2 > 1B/Ag/SiO_2. This is exactly opposite to the order of MG yield of the catalysts (Table 3). Therefore, the MG yield of the xB/Ag/SiO_2 catalysts increased with the decrease in the particle size of silver species.

It was reported that the acidic sites are propitious to the absorption and activation of acyl groups in the hydrogenation process, thereby improving the selectivity of the target product.[30] In our case, the acid amount of the xB/Ag/SiO_2 catalysts increased along with the increase of the B content, as revealed by NH_3-TPD characterization (Figure 8); however, the selectivity of MG did not increase accordingly. This result suggests that the amount of acidic sites is not a critical parameter that determines the MG selectivity of the Ag-based catalyst. This conclusion is inconsistent with that reported by other researchers.[30]

Stability is an important property that determines the practical applicability of a catalyst. Thus, the stability test was carried out on the Ag/SiO_2 and 1B/Ag/SiO_2 catalysts; the results are shown in Figure 12. For the sample of 1B/Ag/SiO_2,

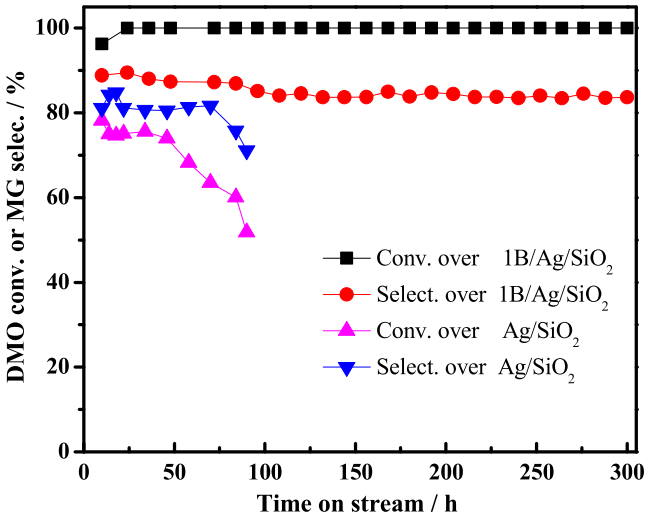

Figure 12. Long-term performance of the Ag/SiO_2 and 1B/Ag/SiO_2 catalysts. Reaction conditions: 493 K, 1.5 MPa, H_2/DMO molar ratio = 150, LHSV = 0.28 h^{-1}.

after ~24 h of "running in" stage of the reaction, the conversion of DMO reached constant, with no sign of deactivation observed after 300 h of reaction, while the selectivity of MG initially decreased slightly from 88.8% (at 12 h) to 85.2% (at 96 h) and then remained constant. Contrarily, the Ag/SiO_2 catalyst presented obvious deactivation within 90 h under identical reaction conditions. It can be concluded that the addition of a suitable amount of B greatly enhanced the catalytic stability of the Ag/SiO_2 catalyst. Moreover, the 1B/Ag/SiO_2 catalyst investigated in the present work shows longer stability under a higher liquid hourly space velocity of 0.28 h^{-1}, compared with the corresponding data (264 h, LHSV = 0.2 h^{-1}) of the Ag−5%B/SiO_2 catalyst reported by Chen et al.[30] The difference may result from the different preparation methods for the Ag/SiO_2 catalyst, in which the impregnation method was used in ref 30, while the ammonia evaporation deposition−precipitation method was adopted in the present work.

The increase in the stability of the Ag/SiO_2 catalyst modified by B can be attributed to the strong interaction between silver and boria, which is supposed to stabilize active silver species and suppress sintering of active metal particles during the reaction process.[25] To verify the supposition, the catalysts after a long-term test were studied by XRD characterization, and the results are shown in Figure 13. The size of Ag crystallites

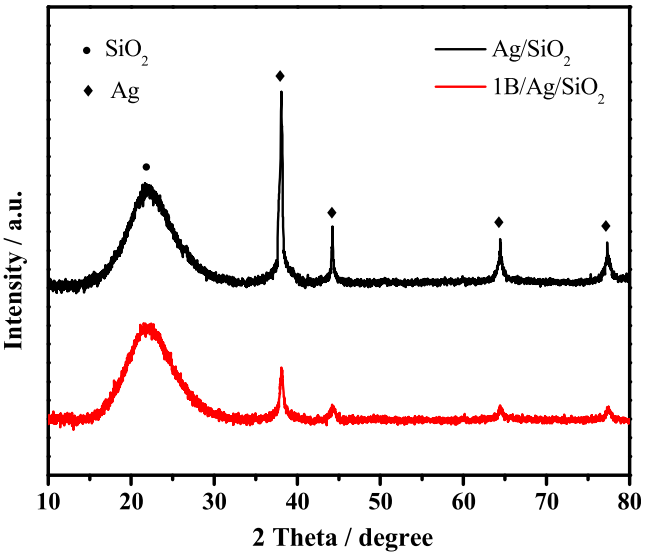

Figure 13. XRD patterns of the Ag/SiO_2 and 1B/Ag/SiO_2 catalysts after reaction testing.

calculated by the Scherrer formula over the Ag/SiO_2 catalyst after a 90 h reaction test was 22.4 nm, which was significantly larger than that of the fresh catalyst (16.9 nm). In contrast, the size of Ag crystallites over the 1B/Ag/SiO_2 catalyst after a 300 h reaction test was 13.3 nm, which was almost identical to that of the fresh catalyst (13.2 nm). These results clearly indicate that the addition of a suitable amount of boron can effectively hinder the sintering and growth of Ag particles, thereby improving the long-term stability of the Ag/SiO_2 catalyst.

The comparison of catalytic performance between the best 1B/Ag/SiO_2 catalyst and the recently reported materials has been listed in Table 5. Note that the experimental conditions used in the literature are different from each other. However, we achieved 100% DMO conversion and 88.3% MG selectivity using the 1B/Ag/SiO_2 catalyst with high stability. In comparison, boron-modified Ag/SiO_2 catalysts seem to be promising, even they still need to be optimized.

3. CONCLUSIONS

In summary, we have studied the effects of B contents on the catalytic performance of B_2O_3-modified Ag/SiO_2 catalysts for the selective hydrogenation of DMO to the MG reaction. The results indicated that with increasing the content of B, the MG yield increased first, passing through a maximum, and then decreased at higher B contents. The xB/Ag/SiO_2 catalyst with 1 wt % B exhibited the highest catalytic activity for the selective

https://doi.org/10.1021/acsomega.2c04880
ACS Omega 2022, 7, 41224−41235

Table 5. Comparison of Performance of Different Catalysts

catalyst	reaction conditions	catalytic performance	reference
Na_2SiO_3 modified Cu/SiO_2	T = 200 °C, P = 2.5 MPa, H_2/DMO = 80 (molar ratio), WLHSV = 1.5 h^{-1}	83% DMO conversion, 99.8% MG selectivity, and can maintain for 6 h	3
B-modified carbon aerogel-supported Cu	T = 230 °C, P = 2.4 MPa, H_2/DMO = 180 (molar ratio), LHSV = 1 h^{-1}	DMO conversion and MG selectivity were 84.6 and 45.2%.	20
Ni_3P/RB-MSN	T = 190 °C, P = 2.5 MPa, H_2/DMO = 90 (molar ratio), WLHSV = 0.44 g^{-1} g_{cat}^{-1} h^{-1}	100% DMO conversion, 85.0% MG selectivity, and can maintain for 500 h	29
Ru/activated carbon	T = 90 °C, P = 3 MPa, H_2/DMO = 260 (molar ratio), WHSV = 0.15 h^{-1}	97.2% DMO conversion, 94.6% MG selectivity, and can maintain for 1032 h	50
P-modifiedCo/SiO_2	T = 240 °C, P = 3 MPa, H_2/DMO = 160 (molar ratio), LHSV = 0.06 h^{-1}	94.6% DMO conversion, 88.1% MG selectivity, and can maintain for 300 h	51
B-modifiedAg/SiO_2 catalysts	T = 220 °C, P = 1.5 MPa, H_2/DMO = 150 (molar ratio), LHSV = 0.28 h^{-1}	100% DMO conversion, 88.3% MG selectivity, and can maintain for 300 h	this work

hydrogenation of DMO to MG, which could be ascribed to the largest amounts of well-dispersed active metal on the catalyst surface. Additionally, the lifespan of the $1B/Ag/SiO_2$ catalyst can be greatly extended to at least 300 h with excellent catalytic behavior at 493 K, 1.5 MPa, and LHSV = 0.28 h^{-1}, which can be attributed to the reduced sintering of Ag for the strong Ag−B interaction. Furthermore, the $1B/Ag/SiO_2$ catalyst prepared by post B modification exhibited significantly higher activity than that of the $Ag-1B/SiO_2$ catalyst prepared by one-step ammonia evaporation deposition−precipitation.

4. EXPERIMENTAL SECTION

4.1. Catalyst Preparation. A commercial silica sol (Qingdao Haiyang Chemicals Company, China) was used as the support in this study. $AgNO_3$ (AR) and H_3BO_3 (AR) were purchased from Shanghai Titan Scientific Co., Ltd. (China) and used as the starting materials.

The Ag/SiO_2 catalyst with a preset silver loading of 10 wt % was prepared by the ammonia evaporation deposition−precipitation method.[38] A typical procedure is as follows. A certain amount of $AgNO_3$ was dissolved in deionized water. Then, an ammonia aqueous solution was added and stirred for 30 min at 60 °C to form a silver ammonia complex solution. Next, a certain amount of silica sol was added to the above silver ammonia complex solution and stirred for another 4 h. The initial pH of the suspension was 11−12. The suspension was then heated to 90 °C and held at this temperature to allow the evaporation of ammonia and the decrease of pH and consequently the deposition of silver species on the silica surface. When the pH value of the suspension was decreased to 7−8, the evaporation process was terminated. The resulting precipitate was washed with deionized water three times, and the obtained filter cake was dried at 120 °C overnight to yield a gray powder of Ag/SiO_2 precursor. B-modified Ag/SiO_2 catalysts were prepared by an incipient wetness impregnation method. An aqueous solution of H_3BO_3 was dropped onto the Ag/SiO_2 precursor in a 100 mL crucible. The slurry was ultrasonically aged for 30 min at room temperature, dried overnight at 120 °C, and then calcined in static air at 350 °C at a temperature rate of 1 °C min^{-1} for 4 h. The obtained catalysts are designed as xB/Ag/SiO_2 (x = 0.5, 1, 3, and 5), where x represents the nominal weight percent of boron.

The $Ag-B/SiO_2$ catalyst with 10 wt % Ag and 1 wt % B was also prepared by the ammonia evaporation deposition−precipitation method, according to the procedure described above for the preparation of the Ag/SiO_2 precursor,[38] in which the aqueous solution contains the desired amounts of $AgNO_3$ and H_3BO_3. Then, the dried powder was calcined in static air at 350 °C for 4 h (heating rate of 1 °C min^{-1}), and the obtained catalyst was designated as $Ag-1B/SiO_2$.

4.2. Catalyst Characterization. The chemical compositions of the as-prepared samples were determined by X-ray fluorescence (XRF) spectroscopy. Catalyst powders were compressed into a self-supporting wafer prior to analysis.

BET specific surface areas (S_{BET}), pore volumes (V_p), and average pore diameters (D_p) of the catalysts were measured by N_2 adsorption−desorption isotherms at −196 °C using a Micromeritics ASAP 2020 HD88 adsorption apparatus after degassing the samples under vacuum at 200 °C for 6 h. S_{BET} was calculated using a value of 0.162 nm^2 for the cross-sectional area of the nitrogen molecule. The total pore volume was derived from the adsorbed N_2 volume at a relative pressure of approximately 0.99, and the Barrett−Joyner−Halenda (BJH) method was used to calculate the pore size distributions according to the desorption branch of the isotherms.

Powder X-ray diffraction (XRD) patterns of the samples were acquired on a PANalytical X'Pert instrument using Ni-filtered Cu Kα radiation at 40 kV and 40 mA. 2θ angles ranged from 10 to 80° with a speed of 4° per minute. Each XRD pattern was identified by matching the results with reference patterns that were included in the JCPDS database. The full width at half-maximum of Ag(111) reflection was measured to calculate the crystallite sizes using the Scherrer equation.

The infrared (IR) spectra were recorded on a Nicolet iZ10 (Thermo Fisher Scientific, American) FTIR spectrophotometer in the range of 400−4000 cm^{-1}. The powder samples were mixed with KBr (2 wt %) and pressed into translucent disks at room temperature.

Transmission electron microscopy (TEM), scanning TEM, and energy-dispersive X-ray spectroscopy mapping (EDX mapping) were conducted on a JEOL JEM 2100F transmission electron microscope working at 200 kV.

Temperature-programmed reduction (TPR) measurements were performed in a linear quartz microreactor. One-hundred milligrams of the sample was purged with N_2 at 200 °C for 2 h to remove adsorbed water and other contaminants. After being cooled down to 30 °C, the catalyst was exposed to 10% H_2/N_2 (30 $cm^3 \cdot min^{-1}$) and heated up to 650 °C at a heating rate of 10 °C min^{-1}. H_2 consumption was monitored by a thermal conductivity detector (TCD).

NH_3-TPD was performed in a continuous flow apparatus equipped with a temperature programmer. One-hundred milligrams of the sample (40−60 mesh) was loaded into a microreactor (linear quartz tube), pretreated at 300 °C in flowing 10% H_2/N_2 for 1 h, and then cooled to 50 °C and fed with NH_3 for 40 min. Afterward, the sample was swept with N_2 at 100 °C for 1 h to purge out the physically adsorbed NH_3.

https://doi.org/10.1021/acsomega.2c04880
ACS Omega 2022, 7, 41224−41235

NH_3 desorption was conducted in flowing N_2 (30 ml/min) by heating up from 100 to 600 °C at 10 °C/min. A gas chromatograph (GC) equipped with a thermal conductivity detector (TCD) was used to continuously monitor the desorbing gas.

X-ray photoelectron spectroscopy (XPS) was performed on an Escalab 250 Xi spectrometer with MgKα radiation (1486.6 eV). The samples were pretreated in situ in a reaction chamber and then transferred to an analysis chamber under vacuum. The binding energy (BE) was calibrated by setting the C 1s peak (BE = 284.6 eV) as a reference. The surface atomic concentrations were quantified by sensitivity factors of the XPS instrument.

4.3. Catalytic Performance Measurement. DMO hydrogenation was carried out using a fixed-bed, stainless-steel tubular reactor. The catalyst (0.5 g; 40−60 mesh) packed between two layers of quartz sand was pretreated in H_2 stream (50 cm^3/min) at 300 °C (heating rate of 1 °C/min) for 4 h and then cooled to the reaction temperature. The reactant (13 wt % DMO/methanol solution) and pure H_2 are fed into the reactor through a series 2PB constant-flux pump (Beijing Xingda Science & Technology Development Co., Ltd., China) with 1.5 MPa system pressure. A Qiyang GC-9860 gas chromatograph equipped with an HP-INNOWAX capillary column (30 m × 0.25 mm × 0.25 μm) and a flame ionization detector (FID) was used for product analysis. The DMO conversion (C_{DMO}) and product selectivity (S_i) were defined as below

$$C_{DMO} = \left(1 - A_{DMO} f_{DMO} / \sum A_i f_i\right) \times 100\% \quad (1)$$

$$S_i = \left(A_i f_i / \sum A_i f_i\right) \times 100\% \quad (2)$$

where A_i represents the peak area of the individual component i in the product stream, and f_i represents the molar correction factor.

The turnover frequency (TOF) was calculated by the below formula[5]

$$\mathrm{TOF} = \frac{C_{DMO} \times X_{DMO} \times V}{D \times N_{Ag}} \quad (3)$$

where C_{DMO} is the DMO concentration in the reactant solution; X_{DMO} is the DMO conversion; V is the flow rate of the reactant solution; D is the Ag dispersion; and N_{Ag} is the the total amount of Ag.

■ ASSOCIATED CONTENT

Supporting Information

The Supporting Information is available free of charge at https://pubs.acs.org/doi/10.1021/acsomega.2c04880.

Additional characterization data and reaction testing data of relevant samples can be found in the Supporting Information (PDF)

■ AUTHOR INFORMATION

Corresponding Authors

Tao Meng − *School of Chemical and Environmental Engineering, Shanghai Institute of Technology, Shanghai 201418, P. R. China*; orcid.org/0000-0003-3477-359X; Phone: +86-21-6087 3301; Email: mengtao@sit.edu.cn

Dongsen Mao − *School of Chemical and Environmental Engineering, Shanghai Institute of Technology, Shanghai 201418, P. R. China*; Email: dsmao@sit.edu.cn

Authors

Shuai Cheng − *School of Chemical and Environmental Engineering, Shanghai Institute of Technology, Shanghai 201418, P. R. China*

Xiaoming Guo − *School of Chemical and Environmental Engineering, Shanghai Institute of Technology, Shanghai 201418, P. R. China*; orcid.org/0000-0002-4912-734X

Jun Yu − *School of Chemical and Environmental Engineering, Shanghai Institute of Technology, Shanghai 201418, P. R. China*; orcid.org/0000-0003-0756-6333

Complete contact information is available at: https://pubs.acs.org/10.1021/acsomega.2c04880

Notes

The authors declare no competing financial interest.

■ ACKNOWLEDGMENTS

The financial support of Shanghai Municipal Science and Technology Commission (20ZR1455500) is gratefully acknowledged.

■ REFERENCES

(1) Ouyang, M. Y.; Wang, Y.; Zhang, J.; Zhao, Y. J.; Wang, S. P.; Ma, X. B. Three dimensional Ag/KCC-1 catalyst with a hierarchical fibrous framework for the hydrogenation of dimethyl oxalate. *RSC Adv.* **2016**, *6*, 12788−12791.

(2) An, J. W.; Wang, X. H.; Zhao, J. X.; Jiang, S. H.; Quan, Y. H.; Pei, Y. L.; Wu, M. M.; Ren, J. Density-functional theory study on hydrogenation of dimethyl oxalate to methyl glycolate over copper catalyst: Effect of copper valence state. *Mol. Catal.* **2020**, *482*, No. 110667.

(3) Huang, H. J.; Wang, B.; Wang, Y.; Zhao, Y. J.; Wang, S. P.; Ma, X. B. Partial hydrogenation of dimethyl oxalate on Cu/SiO_2 catalyst modified by sodium silicate. *Catal. Today* **2020**, *358*, 68−73.

(4) Zhu, J.; Cao, L. Q.; Li, C. Y.; Zhao, G. F.; Zhu, T.; Hu, W.; Sun, W. D.; Lu, Y. Nanoporous Ni_3P evolutionarily structured onto a Ni foam for highly selective hydrogenation of dimethyl oxalate to methyl glycolate. *ACS Appl. Mater. Interfaces* **2019**, *11*, 37635−37643.

(5) Zhou, J. F.; Duan, X. P.; Ye, L. M.; Zheng, J. W.; Li, M. M. J.; Tsang, S. C. E.; Yuan, Y. Z. Enhanced chemoselective hydrogenation of dimethyl oxalate to methyl glycolate over bimetallic Ag−Ni/SBA-15 catalysts. *Appl. Catal. A* **2015**, *505*, 344−353.

(6) Wang, B. W.; Xu, Q.; Song, H.; Xu, G. H. Synthesis of methyl glycolate by hydrogenation of dimethyl oxalate over $Cu\text{-}Ag/SiO_2$ catalyst. *J. Nat. Gas Chem.* **2007**, *16*, 78−80.

(7) He, D. H.; Huang, W. G.; Liu, J. Y.; Zhu, Q. M. Condensation of formaldehyde and methyl formate to methyl glycolate and methyl methoxy acetate using heteropolyacids and their salts. *Catal. Today* **1999**, *51*, 127−134.

(8) Abbas, M.; Chen, Z.; Zhang, J.; Chen, J. G. Highly dispersed, ultra-small and noble metal-free Cu nanodots supported on porous SiO_2 and their excellent catalytic hydrogenation of dimethyl oxalate to methyl glycolate. *New J. Chem.* **2018**, *42*, 10290−10299.

(9) Dong, G. L.; Luo, Z. W.; Cao, Y. Q.; Zheng, S. N.; Zhou, J. H.; Li, W.; Zhou, X. G. Understanding size-dependent hydrogenation of dimethyl oxalate to methyl glycolate over Ag catalysts. *J. Catal.* **2021**, *401*, 252−261.

(10) Chen, H. M.; Tan, J. J.; Zhu, Y. L.; Li, Y. W. An effective and stable Ni_2P/TiO_2 catalyst for the hydrogenation of dimethyl oxalate to methyl glycolate. *Catal. Commun.* **2016**, *73*, 46−49.

(11) Chen, Y. F.; Han, L. P.; Zhu, J.; Chen, P. J.; Fan, S. Y.; Zhao, G. F.; Liu, Y.; Lu, Y. High-performance $Ag\text{-}CuO_x$ nanocomposite catalyst

galvanically deposited onto a Ni-foam for gas-phase dimethyl oxalate hydrogenation to methyl glycolate. *Catal. Commun.* **2017**, *96*, 58−62.
(12) Abbas, M.; Zhang, J.; Chen, J. G. Sonochemical engineering of highly efficient and robust Au nanoparticle-wrapped on Fe/ZrO_2 nanorods and their controllable product selectivity in dimethyl oxalate hydrogenation. *Catal. Sci. Technol.* **2020**, *10*, 1125−1134.
(13) Li, M. M. J.; Ye, L. M.; Zheng, J. W.; Fang, H. H.; Kroner, A.; Yuan, Y. Z.; Tsang, S. C. E. Surfactant-free nickel−silver core@shell nanoparticles in mesoporous SBA-15 for chemoselective hydrogenation of dimethyl oxalate. *Chem. Commun.* **2016**, *52*, 2569−2572.
(14) Duan, X. P.; Chen, T. Y.; Chen, T. X.; Huang, L. L.; Ye, L.; Lo, B. T. W.; Yuan, Y. Z.; Tsang, S. C. E. Intercalating lithium into the lattice of silver nanoparticles boosts catalytic hydrogenation of carbon−oxygen bonds. *Chem. Sci.* **2021**, *12*, 8791−8802.
(15) Zhao, Y. J.; Zhang, Y. Q.; Wang, Y.; Zhang, J.; Xu, Y.; Wang, S. P.; Ma, X. B. Structure evolution of mesoporous silica supported copper catalyst for dimethyl oxalate hydrogenation. *Appl. Catal. A* **2017**, *539*, 59−69.
(16) Ai, P. P.; Tan, M. H.; Ishikuro, Y.; Hosoi, Y.; Yang, G. H.; Yoneyama, Y.; Tsubaki, N. Design of an autoreduced copper in carbon nanotube catalyst to realize the precisely selective hydrogenation of dimethyl oxalate. *ChemCatChem* **2017**, *9*, 1067−1075.
(17) Wang, B.; Cui, Y. Y.; Wen, C.; Chen, X.; Dong, Y.; Dai, W. L. Role of copper content and calcination temperature in the structural evolution and catalytic performance of Cu/P25 catalysts in the selective hydrogenation of dimethyl oxalate. *Appl. Catal. A* **2016**, *509*, 66−74.
(18) He, L. M.; Chen, X. C.; Ma, J. S.; He, H. L.; Wang, W. Characterization and catalytic performance of sol−gel derived Cu/SiO_2 catalysts for hydrogenolysis of diethyl oxalate to ethylene glycol. *J. Sol−Gel Sci. Technol.* **2010**, *55*, 285−292.
(19) Cui, Y. Y.; Wang, B.; Wen, C.; Chen, X.; Dai, W. L. Investigation of activated-carbon-supported copper catalysts with unique catalytic performance in the hydrogenation of dimethyl oxalate to methyl glycolate. *ChemCatChem* **2016**, *8*, 527−531.
(20) Lu, X. D.; Wang, G. F.; Yang, Y.; Kong, X. P.; Chen, J. G. A boron-doped carbon aerogel-supported Cu catalyst for the selective hydrogenation of dimethyl oxalate. *New J. Chem.* **2020**, *44*, 3232−3240.
(21) Yin, A. Y.; Guo, X. Y.; Dai, W. L.; Fan, K. N. High activity and selectivity of Ag/SiO_2 catalyst for hydrogenation of dimethyl oxalate. *Chem. Commun.* **2010**, *46*, 4348−4350.
(22) Yin, A. Y.; Wen, C.; Dai, W. L.; Fan, K. N. Ag/MCM-41 as a highly efficient mesostructured catalyst for the chemoselective synthesis of methyl glycolate and ethylene glycol. *Appl. Catal. B* **2011**, *108-109*, 90−99.
(23) Hu, M. L.; Yan, Y.; Duan, X. P.; Ye, L. M.; Zhou, J. F.; Lin, H. Q.; Yuan, Y. Z. Effective anchoring of silver nanoparticles onto N-doped carbon with enhanced catalytic performance for the hydrogenation of dimethyl oxalate to methyl glycolate. *Catal. Commun.* **2017**, *100*, 148−152.
(24) Zheng, J. W.; Lin, H. Q.; Zheng, X. L.; Duan, X. P.; Yuan, Y. Z. Highly efficient mesostructured Ag/SBA-15 catalysts for the chemoselective synthesis of methyl glycolate by dimethyl oxalate hydrogenation. *Catal. Commun.* **2013**, *40*, 129−133.
(25) Zheng, J. W.; Duan, X. P.; Lin, H. Q.; Gu, Z. Q.; Fang, H. H.; Li, J. H.; Yuan, Y. Z. Silver nanoparticles confined in carbon nanotubes: on the understanding of the confinement effect and promotional catalysis for the selective hydrogenation of dimethyl oxalate. *Nanoscale* **2016**, *8*, 5959−5967.
(26) Ouyang, M. Y.; Wang, J.; Peng, B.; Zhao, Y. J.; Wang, S. P.; Ma, X. B. Effect of Ti on Ag catalyst supported on spherical fibrous silica for partial hydrogenation of dimethyl oxalate. *Appl. Surf. Sci.* **2019**, *466*, 592−600.
(27) Wen, C.; Cui, Y. Y.; Chen, X.; Zong, B. N.; Dai, W. L. Reaction temperature controlled selective hydrogenation of dimethyl oxalate to methyl glycolate and ethylene glycol over copper-hydroxyapatite catalysts. *Appl. Catal. B* **2015**, *162*, 483−493.
(28) Abbas, M.; Chen, Z.; Chen, J. G. Shape- and size-controlled synthesis of Cu nanoparticles wrapped on RGO nanosheet catalyst and their outstanding stability and catalytic performance in the hydrogenation reaction of dimethyl oxalate. *J. Mater. Chem. A* **2018**, *6*, 19133−19142.
(29) Zhao, G. F.; Li, H.; Si, J. Q.; Nie, Q.; Meng, C.; Liu, Y.; Lu, Y. High-performance Ni_3P/meso-SiO_2 for gas-phase hydrogenation of dimethyl oxalate to methyl glycolate. *ACS Sustainable Chem. Eng.* **2021**, *9*, 16719−16729.
(30) Chen, H. M.; Tan, J. J.; Cui, J. L.; Yang, X. H.; Zheng, H. Y.; Zhu, Y. L.; Li, Y. W. Promoting effect of boron oxide on Ag/SiO_2 catalyst for the hydrogenation of dimethyl oxalate to methyl glycolate. *Mol. Catal.* **2017**, *433*, 346−353.
(31) Zheng, J. W.; Lin, H. Q.; Wang, Y. N.; Zheng, X. L.; Duan, X. P.; Yuan, Y. Z. Efficient low-temperature selective hydrogenation of esters on bimetallic Au−Ag/SBA-15 catalyst. *J. Catal.* **2013**, *297*, 110−118.
(32) He, Z.; Lin, H. Q.; He, P.; Yuan, Y. Z. Effect of boric oxide doping on the stability and activity of a $Cu-SiO_2$ catalyst for vapor-phase hydrogenation of dimethyl oxalate to ethylene glycol. *J. Catal.* **2011**, *277*, 54−63.
(33) Zhao, S.; Yue, H. R.; Zhao, Y. J.; Wang, B.; Geng, Y. C.; Lv, J.; Wang, S. P.; Gong, J. L.; Ma, X. B. Chemoselective synthesis of ethanol via hydrogenation of dimethyl oxalate on Cu/SiO_2: Enhanced stability with boron dopant. *J. Catal.* **2013**, *297*, 142−150.
(34) Yang, D. L.; Ye, R. P.; Lin, L.; Guo, R.; Zhao, P. Y.; Yin, Y. C.; Cheng, W.; Yuan, W. P.; Yao, Y. G. Boron modified bifunctional Cu/SiO_2 catalysts with enhanced metal dispersion and surface acid sites for selective hydrogenation of dimethyl oxalate to ethylene glycol and ethanol. *Nanomaterials* **2021**, *11*, 3236.
(35) Yin, A. Y.; Qu, J. W.; Guo, X. Y.; Dai, W. L.; Fan, K. N. The influence of B-doping on the catalytic performance of Cu/HMS catalyst for the hydrogenation of dimethyloxalate. *Appl. Catal. A* **2011**, *400*, 39−47.
(36) Takahashi, R.; Sato, S.; Sodesawa, T.; Kato, M.; Yoshida, S. Preparation of Cu/SiO_2 catalyst by solution exchange of wet silica gel. *J. Sol−Gel Sci. Technol.* **2000**, *19*, 715−718.
(37) Chen, Y.; Liu, Y. M.; Mao, D. S.; Yu, J.; Zheng, Y. L.; Guo, X. M.; Ma, Z. Facile cyclodextrin-assisted synthesis of highly active CuO-CeO_2/MCF catalyst for CO oxidation. *J. Taiwan Inst. Chem. Eng.* **2020**, *113*, 16−26.
(38) Cheng, S.; Mao, D. S.; Guo, X. M.; Yu, J. Synthesis of methyl glycolate from the hydrogenation of dimethyl oxalate on Ag/SiO_2 catalyst: the effects of Ag contents and promoters. *React. Kinet. Mech. Catal.* **2019**, *126*, 1067−1079.
(39) Zhu, Y. Y.; Wang, S. R.; Zhu, L. J.; Ge, X. L.; Li, X. B.; Luo, Z. Y. The influence of copper particle dispersion in Cu/SiO_2 catalysts on the hydrogenation synthesis of ethylene glycol. *Catal. Lett.* **2010**, *135*, 275−281.
(40) Sloczynski, J.; Grabowski, R.; Olszewski, P.; Kozłowska, A.; Stoch, J.; Lachowska, M.; Skrzypek, J. Effect of metal oxide additives on the activity and stability of $Cu/ZnO/ZrO_2$ catalysts in the synthesis of methanol from CO_2 and H_2. *Appl. Catal. A* **2006**, *310*, 127−137.
(41) Witoon, T.; Lapkeatseree, V.; Numpilai, T.; Kui Cheng, C.; Limtrakul, J. CO_2 hydrogenation to light olefins over mixed Fe-Co-K-Al oxides catalysts prepared via precipitation and reduction methods. *Chem. Eng. J.* **2022**, *428*, No. 131389.
(42) Huang, Z. W.; Cui, F.; Kang, H. X.; Chen, J.; Zhang, X. Z.; Xia, C. G. Highly dispersed silica-supported copper nanoparticles prepared by precipitation−gel method: A simple but efficient and stable catalyst for glycerol hydrogenolysis. *Chem. Mater.* **2008**, *20*, 5090−5099.
(43) Neumair, S. C.; Kaindl, R.; Hoffmann, R.-D.; Huppertz, H. The new high-pressure borate hydrate $Cu_3B_6O_{12}{\cdot}H_2O$. *Solid State Sci.* **2012**, *14*, 229−235.
(44) Sitarz, M.; Handke, M.; Mozgawa, W. Identification of silicooxygen rings in SiO_2 based on IR spectra. *Spectrochim. Acta, Part A* **2000**, *56*, 1819−1823.

https://doi.org/10.1021/acsomega.2c04880
ACS Omega 2022, 7, 41224−41235

(45) Yang, G. Q.; Han, B.; Sun, Z. T.; Yan, L. M.; Wang, X. Y. Preparation and characterization of brown nanometer pigment with spinel structure. *Dyes Pigments* **2002**, *55*, 9−16.
(46) Cheng, S.; Meng, T.; Mao, D. S.; Guo, X. M.; Yu, J.; Ma, Z. Ni-modified Ag/SiO_2 catalysts for selective hydrogenation of dimethyl oxalate to methyl glycolate. *Nanomaterials* **2022**, *12*, 407.
(47) Chen, X. F.; Li, H. X.; Luo, H. S.; Qiao, M. H. Liquid phase hydrogenation of furfural to furfuryl alcohol over Mo-doped Co-B amorphous alloy catalysts. *Appl. Catal. A* **2002**, *233*, 13−20.
(48) Zhu, S. H.; Gao, X. Q.; Zhu, Y. L.; Zhu, Y. F.; Zheng, H. Y.; Li, Y. W. Promoting effect of boron oxide on Cu/SiO_2 catalyst for glycerol hydrogenolysis to 1,2-propanediol. *J. Catal.* **2013**, *303*, 70−79.
(49) Wang, Y.; Zheng, J. M.; Fan, K. N.; Dai, W. L. One-pot solvent-free synthesis of sodium benzoate from the oxidation of benzyl alcohol over novel efficient AuAg/TiO_2 catalysts. *Green Chem.* **2011**, *13*, 1644−1647.
(50) Zheng, H. Y.; Xue, Y. F.; Niu, Y. L.; Gao, X. Q.; Wang, Y. Q.; Ding, G. Q.; Zhu, Y. L. Synthesis of methyl glycolate via low-temperature hydrogenation of dimethyl oxalate over an efficient and stable Ru/activated carbon catalyst. *J. Chem. Technol. Biotechnol.* **2022**, *97*, 2572−2580.
(51) Zhuang, Z. L.; Li, Y. H.; Chen, F.; Chen, X. K.; Li, Z.; Wang, S. Y.; Wang, X. P.; Zhu, H. J.; Tan, Y.; Ding, Y. J. Synthesis of methyl glycolate by hydrogenation of dimethyl oxalate with a P modified Co/SiO2 catalyst. *Chem. Commun.* **2022**, *58*, 1958−1961.

https://doi.org/10.1021/acsomega.2c04880
ACS Omega 2022, 7, 41224−41235